PHYSICAL REVIEW B VOLUME 25, NUMBER 3 1 FEBRUARY 1982

Oxidation of cobalt and iron near the $\epsilon \rightarrow \gamma$ and $\alpha \rightarrow \gamma$ structural phase transitions

A. L. Cabrera,* B. C. Sales, and M. B. Maple

Institute for Pure and Applied Physical Sciences, University of California, San Diego, La Jolla, California 92093

(Received 23 March 1981)

The oxidation rates of cobalt and iron as a function of oxide thickness and temperature have been measured in the vicinity of the hcp→fcc($\epsilon \rightarrow \gamma$) and bcc→fcc($\alpha \rightarrow \gamma$) crystallographic-phase-transition temperatures using a gravimetric technique. The oxidation rate of both metals changed markedly at the structural-phase-transition temperature. The effects of a crystallographic versus a magnetic phase change on the oxidation rates are compared.

I. INTRODUCTION

During the past several years there has been increasing interest in the effects of electronic, structural, and magnetic phase transitions of a substrate on chemical reactions occurring at or near its surface.[1–17] Much of this work focused on the relationship between the rate of metallic oxidation and the magnetic phase of the metal.[1–7] We have previously investigated the oxidation kinetics of nickel[4,5] and iron[7] in the vicinity of the ferromagnetic to paramagnetic phase transition temperature, T_c. For both metals we observed a relatively large change in the oxidation rate near T_c, as well as a rather unusual dependence of the size of the oxidation rate anomaly on the oxide thickness. In particular, the relative magnitude of the change in the oxidation rate near T_c increased with increasing oxide thickness for both iron and nickel. Hence, it was hoped that a study of the effects of a crystallographic phase transition on the oxidation kinetics of iron and cobalt would yield more information concerning the coupling mechanisms between the bulk characteristics of a metal and its oxidation rate and provide a comparison between the effects of a magnetic versus a crystallographic phase change on the oxidation rate.

In this paper, we present the results of a gravimetric study of the oxidation of cobalt near the ϵ-γ structural phase transition and the oxidation of iron near the $\alpha \rightarrow \gamma$ structural phase transition. The ϵ-γ transition of cobalt is from a hexagonal close packed (hcp) structure (ϵ phase) to a higher temperature face centered cubic (fcc) structure (γ phase) at a temperature $T_{\epsilon-\gamma} \cong 713$ K. The α-γ transition of iron is from a body centered cubic (bcc) structure (α phase) to a higher-temperature fcc structure (γ phase) which occurs at a temperature $T_{\alpha-\gamma} \cong 1190$ K.

II. EXPERIMENTAL DETAILS

A. Cobalt studies

24 pieces of 99.999% pure cobalt foil obtained from Electronic Space Industries were cut into rectangular shapes measuring $0.05 \times 12.5 \times 40$ mm^3. Each cobalt piece was wound into the shape of a spiral and suspended with a Pt hook from one side of a Cahn RG microbalance. It was found that the most reproducible results were obtained if an unexposed cobalt sample was used for each isotherm. The surface of the cobalt was cleaned *in situ* by alternately oxidizing for 20 min then reducing in pure H_2 for 30 min at $T = 628$ K. This procedure was repeated twice before the temperature was increased and the oxidation isotherm was recorded.

Below $T_{\epsilon-\gamma}$ the free energies of the two crystal structures are about equal. This means a variety of factors such as strain induced by cold working or surface effects can alter the approach to equilibrium. At room temperature, for example, about half of a powdered cobalt sample which is cooled through $T_{\epsilon-\gamma}$ remains in the high-temperature cubic phase.[18] For this reason a piece of the cobalt foil used was x rayed after the hydrogen-oxygen pretreatment described above. At room temperature the crystal structure was found to be mainly hcp with only one or two weak x-ray lines belonging to the cubic phase.

B. Iron studies

20 iron spheres each weighing 49 ± 1 mg were prepared from iron of 99.999% purity obtained from Electronic Space Industries by arc melting in an argon atmosphere. Each iron sphere was placed in a small quartz cup and suspended from the microbalance.

Before an oxidation isotherm was recorded, each iron sphere was treated in oxygen and hydrogen in a manner similar to that used for cobalt but at a higher temperature of 972 K.

Because of the way in which oxygen is introduced into the microbalance chamber, during the first minute of an oxidation isotherm the partial pressure of oxygen rapidly changes from 0 to 1 atm. These data are therefore excluded from further analysis. Additional details of the experimental apparatus, the techniques employed to record the oxidation isotherms (weight gain of a metal due to oxidation versus time at a fixed temperature), and the *in situ* calibration of the alumel-chromel thermocouples are given in Ref. 5.

III. RESULTS

A. Cobalt

Several typical oxidation isotherms from 642 to 779 K are shown in Fig. 1. The average oxide thickness x was calculated from the geometric surface area of each piece of cobalt foil assuming that only stoichiometric CoO was formed.[19]

Many theoretical models for metallic oxidation have been suggested in the literature, which, after various approximations, give rise to parabolic, cubic, quartic, linear, direct logarithmic, inverse logarithmic, and double logarithmic oxide growth laws.[20–24] If one considers data from a narrow time or temperature interval, or from a limited range of oxide thicknesses, several of the above rate laws provide an adequate description of the measured oxidation isotherms. However, none of these laws accurately describe the entire collection of isotherms for either Fe or Co. Hence rather than force these data to fit a particular theoretical model, we prefer to use a function which gives an accurate analytic representation of each isotherm.

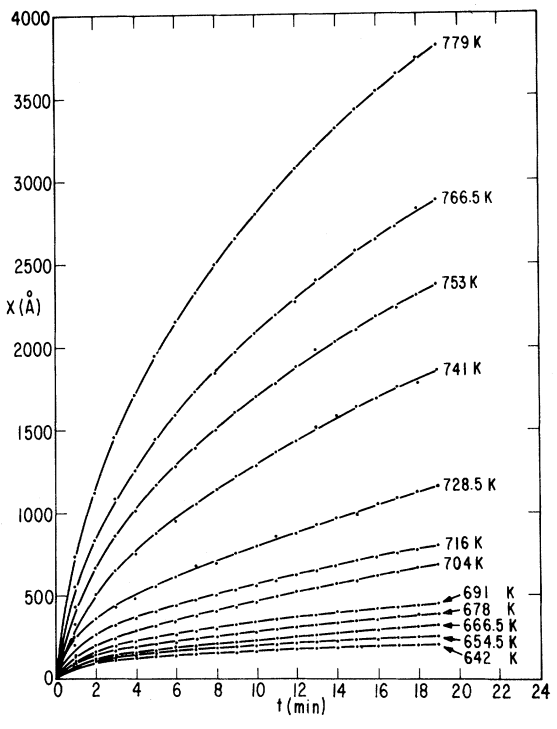

FIG. 1. Typical oxide thickness x vs t isotherms for cobalt oxidation at various temperatures near $T_{\epsilon-\gamma}$.

As was also found in our previous studies of the oxidation kinetics of nickel[4,5] and iron[7] near their magnetic transformation temperatures, a simple power law of the form

$$x = A\left(\frac{t}{t_0}\right)^{\alpha} \tag{1}$$

provides a sufficiently flexible expression to accurately describe both the cobalt and iron oxidation data reported in this paper.[25] In Eq. (1), x is the average oxide thickness in Å, t is the time in minutes, t_0 was taken to be 1 min, and the factor A and the exponent α depend on temperature. For times between 1 and 19 min, each isotherm was fitted by the method of least squares with a line of the form:

$$\ln x = \ln A + \alpha \ln(t/t_0) \ . \tag{2}$$

The isotherms of Fig. 1 are displayed in Fig. 2 as plots of $\log x$ versus $\log t$. For all of the isotherms, the correlation coefficient was better than 0.999 and the reproducibility of A and α was within $\pm 2\%$ and $\pm 3\%$, respectively.

The temperature dependence of the factor A and the exponent α [Eq. (1)] are shown in Fig. 3. As a function of temperature the exponent α increases from a value of 0.35 at 642 K to a maximum of 0.58 at 753 K, then decreases slightly to 0.55 at 779 K. Since A is the amount of oxide which forms on the cobalt surface after 1 min of oxidation, $A/1$ min can be regarded as an average oxidation rate for the 0–1-min time interval. Therefore, $\log A$ versus $1/T$ is plotted in Fig. 3(b). When plotted in this fashion the factor A can be described by two Arrhenius laws. For $T < T_{\epsilon-\gamma}$, $A(T) = A_0 \exp(-E_0/RT)$ where $A_0 = 8.58 \times 10^4$ Å and $E_0 = 9.0 \pm 0.3$ kcal/mole, while for $T > T_{\epsilon-\gamma}$, $A(T) = A_1 \exp(-E_1/RT)$, where $A_1 = 7.55 \times 10^9$ Å and $E_1 = 24.9 \pm 0.2$ kcal/mole.

To determine the effects of the crystallographic phase transition of Co (and Fe) on its oxidation rate, the rate for each oxidation isotherm should be compared in a region where the oxidation mechanism is the same. Since the proposed mechanisms for oxide growth (cation diffusion, electric field assisted cation diffusion, electron tunneling, electron diffusion, etc.) only apply for a limited range of oxide thicknesses, a

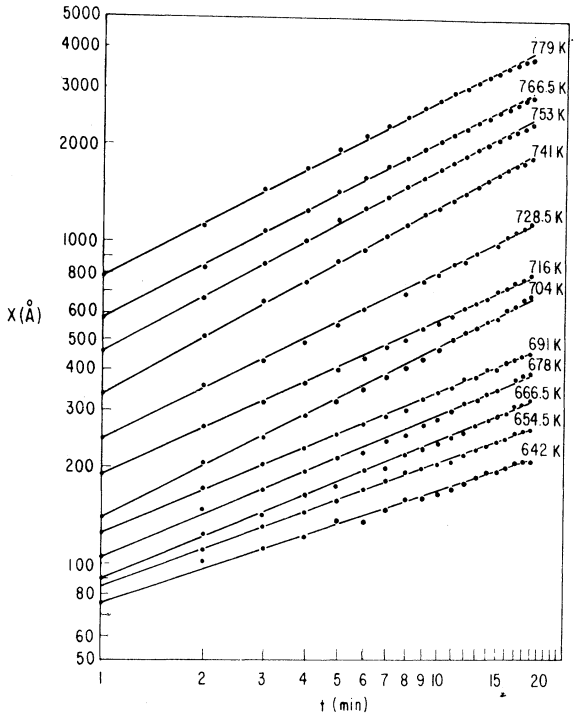

FIG. 2. Typical logarithm of the oxide thickness x vs logarithm of the time t plots for cobalt oxidation at various temperatures near $T_{\epsilon-\gamma}$.

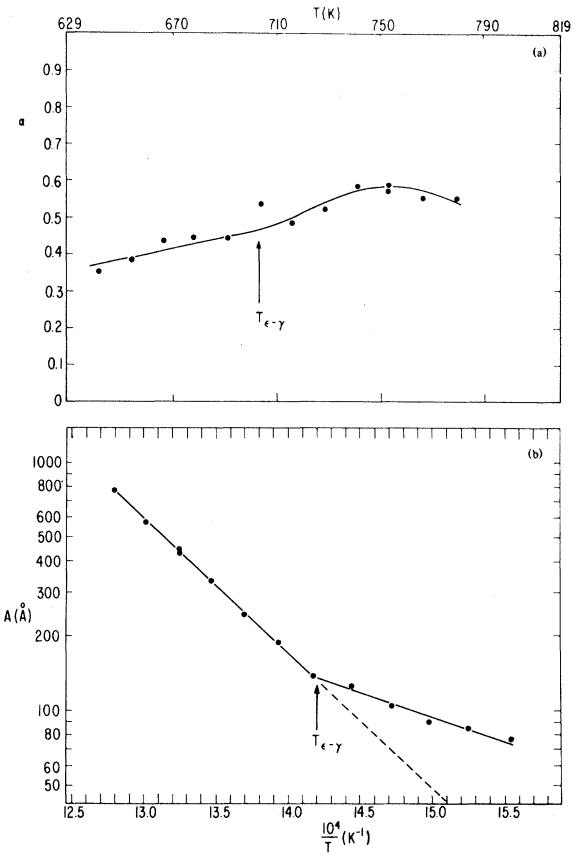

FIG. 3. (a) Exponent α vs absolute temperature T and (b) logarithm of the factor A vs inverse absolute temperature for Co oxidation.

reasonable definition of the oxidation rate is the rate of oxide growth at a fixed oxide thickness x_0. We note that although this definition of the oxidation rate is not unique, it is a physical definition which can be used regardless of the particular oxide growth law encountered.

The oxidation rate r is therefore defined as

$$r = \left.\frac{dx}{dt}\right|_{x_0} = \frac{A\alpha}{t_0}\left(\frac{t}{t_0}\right)^{\alpha-1}\Bigg|_{x=x_0} = \frac{A\alpha}{t_0}\left(\frac{x_0}{A}\right)^{(\alpha-1)/\alpha} . \tag{3}$$

To obtain an accurate derivative, the oxide thickness x_0 should be attained some time between 1 and 19 min (see Fig. 2) since it is only within this interval that the rate [Eq. (3)] is not an extrapolation. This limits the choices for x_0 from about 50–1000 Å.

The rates of oxidation for $x_0 = 50$, 100, 200, and 500 Å are displayed in Fig. 4 as log r versus $1/T$. At $T_{\epsilon-\gamma} \cong 710$ K, there is a definite change in the oxidation rates which becomes smaller for larger oxide thicknesses (larger x_0). These data can be described by $r = r_0 \exp(-E_0/RT)$ for $T < T_{\epsilon-\gamma}$ and by $r = r_1 \exp(-E_1/RT)$ for $T > T_{\epsilon-\gamma}$. The values for r_0, E_0, r_1, and E_1 at various oxide thicknesses are determined by the method of least squares are given in Table I.

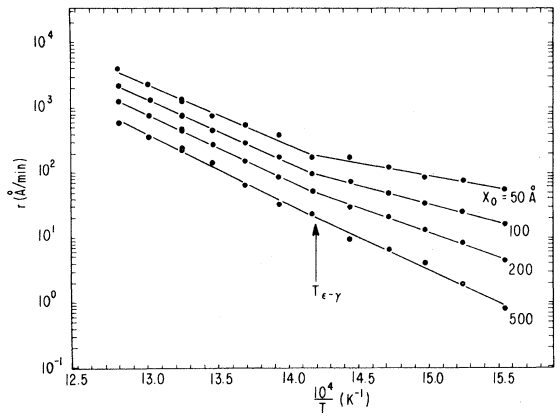

FIG. 4. Logarithm of Co oxidation rate near $T_{\epsilon-\gamma}$ vs inverse absolute temperature for four oxide thicknesses x_0.

TABLE I. Cobalt oxidation parameters for four oxide thicknesses.

x_0 (Å)	E_1 (kcal/mole)	r_1 (10^{15} Å/min)	E_0 (kcal/mole)	r_0 (10^7 Å/min)
50	42.4±1.1	2.75	17.7±0.9	6.42
100	44.6±0.4	7.14	26.4±0.3	1.56×10^3
200	46.7±0.3	15.91	35.1±0.5	4.28×10^5
500	49.5±1.1	51.57	46.4±1.3	5.79×10^8

At this point we must emphasize that the activation energies and prefactors derived from the two Arrhenius laws are not meant to be used quantitatively. As will be discussed in more detail later, the analysis of rate data of any type from such a narrow temperature interval in terms of two Arrhenius laws is questionable. However, in the absence of a specific theory, this method of analysis does provide a simple way of displaying the qualitative changes in the oxidation rate due to the phase transition.

B. Iron

Several typical oxidation isotherms from 1095 to 1230 K are shown in Fig. 5. The average oxide thickness x was calculated from the geometric surface area of each sphere assuming that stoichiometric FeO was formed.[26] The reproducibility of each isotherm was within ±2%.

The analysis of the iron isotherms and the definition of the oxidation rate were identical to those used for the cobalt data. As before, the oxidation isotherms are well described by a power law [Eq. (1)] and for times between 1 and 3.67 min each isotherm was fitted by the method of least squares by Eq. (2). The isotherms of Fig. 5 are displayed as plots of $\log x$ versus $\log t$ in Fig. 6. For all isotherms the correlation coefficient was better than 0.999 and the reproducibility of A and α was within ±2% and ±3%, respectively.

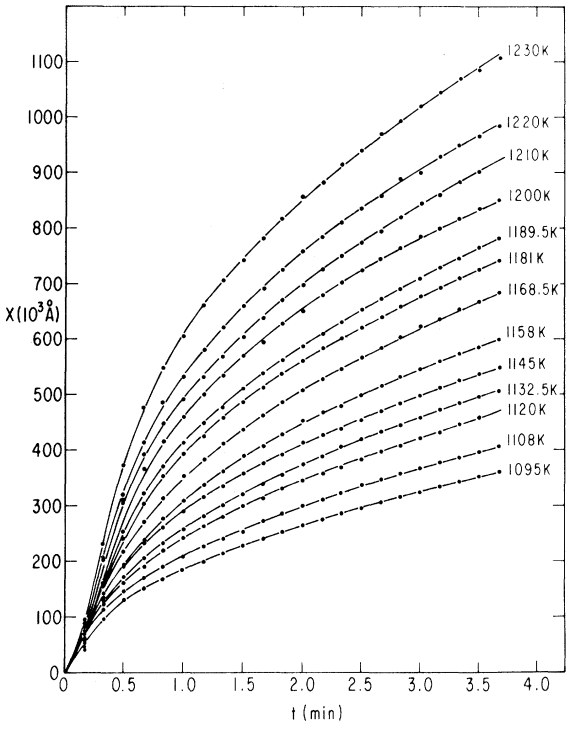

FIG. 5. Typical oxide thickness x vs time t isotherms for iron oxidation at various temperatures near $T_{\alpha-\gamma}$.

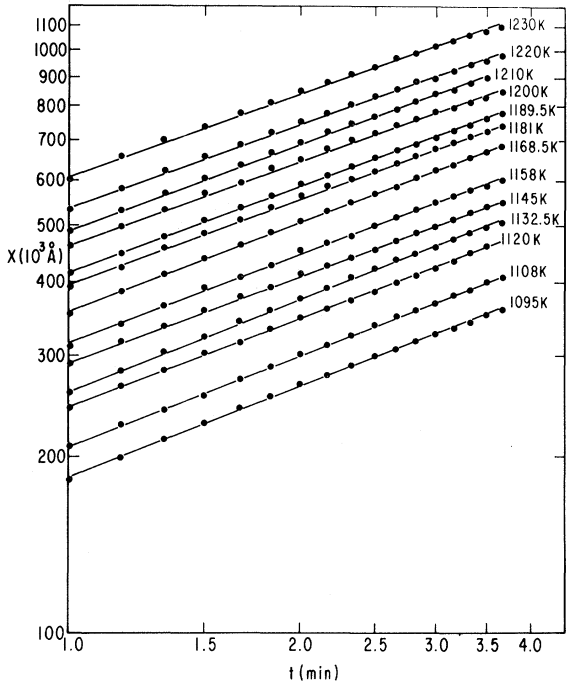

FIG. 6. Typical logarithm of the oxide thickness x vs logarithm of the time t plots for iron oxidation at various temperatures near $T_{\alpha-\gamma}$.

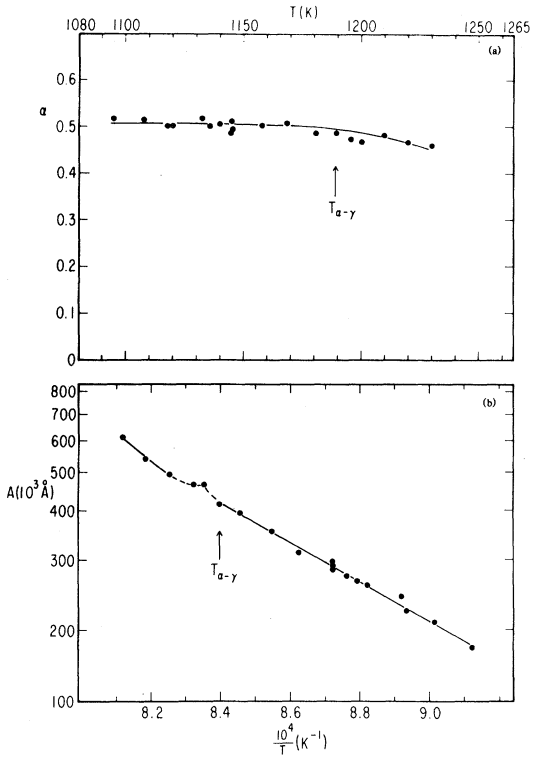

FIG. 7. (a) Exponent α vs absolute temperature T and (b) logarithm of the factor A vs inverse absolute temperature for Fe oxidation.

The temperature dependence of the factor A and the exponent α of Eq. (1) are shown in Fig. 7. The exponent α is approximately constant and is equal to 0.500 ± 0.015 in the temperature range 1095–1168.5 K and then decreases slightly from 0.49 at 1181 K to 0.46 at 1230 K. The factor A can be described by

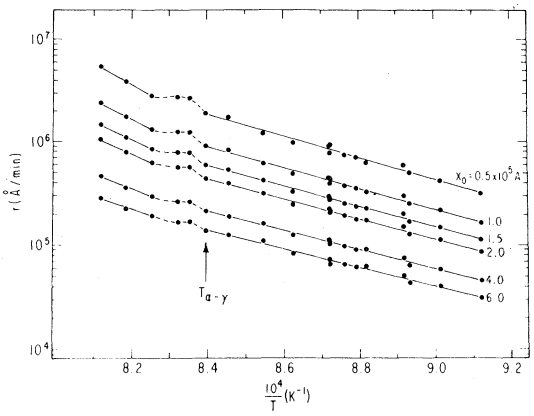

FIG. 8. Logarithm of Fe oxidation rate near $T_{\alpha-\gamma}$ vs inverse absolute temperature for six oxide thicknesses x_0.

$A = A_0 \exp(-E_0/RT)$ for $T < T_{\alpha-\gamma}$ where $A_0 = 6.5 \times 10^9$ Å and $E_0 = 22.8 \pm 0.3$ kcal/mole and by $A = A_1 \exp(-E_1/RT)$ for $T > 1200 > T_{\alpha-\gamma}$ where $A_1 = 2.8 \times 10^{11}$ Å and $E_1 = 31.9 \pm 1.7$ kcal/mole. For temperatures near the $\alpha - \gamma$ transition ($T \sim 1190$ K), A exhibits a small cusplike feature.

The oxidation rate is defined to be the rate of oxide growth at a fixed oxide thickness x_0 [see Eq. (3)]. The rate of oxidation for $x_0 = 0.5$, 1.0, 1.5, 2.0, 4.0, and 6.0×10^5 Å is shown in Fig. 8. As was found for cobalt near $T_{\epsilon-\gamma}$, the change in the oxidation rate of iron near $T_{\alpha-\gamma}$ becomes smaller with increasing oxide thickness x_0. The oxidation rate data for iron can be described by $r = r_0 \exp(-E_0/RT)$ for $T < T_{\alpha-\gamma}$ and by $r = r_1 \exp(-E_1/RT)$ for $T > T_{\alpha-\gamma}$. The values of r_0, E_0, r_1, and E_1 for iron at various oxide thicknesses as determined by the method of least squares are given in Table II.

TABLE II. Iron oxidation parameters for six oxide thicknesses.

x_0 (10^5 Å)	E_1 (kcal/mole)	r_1 (10^{16} Å/min)	E_0 (kcal/mole)	r_0 (10^{12} Å/min)
0.5	97.5±1.2	1.15×10^8	48.6±0.9	1.60×10^3
1.0	86.9±2.2	6.56×10^5	46.7±0.7	341.9
1.5	80.6±2.8	3.16×10^3	45.5±0.6	138.2
2.0	76.2±3.2	3.71×10^3	44.7±0.5	72.9
4.0	65.6±4.3	21.0	42.8±0.5	15.6
6.0	59.4±4.9	1.02	41.6±0.6	6.2

IV. DISCUSSION

A. Previous work

The oxidation of cobalt near the ϵ-γ crystallographic-phase transition has been investigated previously by Chattopadhyay and Measor[8] using a manometric technique. They fitted each isotherm by a logarithmic growth law of the form $x = K_0 \log_{10}(1 + t/\tau)$ and found an anomaly in the logarithmic rate constant K_0, near $T_{\epsilon-\gamma}$. Although the oxidation isotherms reported here are better described by a power law [Eq. (1)], it can be shown that for $642 < T < 779$ K, the prefactor A of the power law is approximately proportional to K_0.

For $T > T_{\epsilon-\gamma}$, the activation energy of A was found to be 24.9 ± 0.2 kcal/mole [see Fig. 3(b)] in good agreement with the value for K_0 of 20 kcal/mole reported by Chattopadhyay and Measor.[8] Because of experimental limitations, the lowest temperature at which we could accurately study the oxidation rates of cobalt was about 640 K. Over the temperature interval from 640 K $< T < T_{\epsilon-\gamma} \cong 700$ K, the prefactor A follows an Arrhenius law with an activation energy of about 9 kcal/mole [see Fig. 3(b)]. Over a similar temperature range, the logarithmic rate constant K_0 can also be described by an Arrhenius law with an activation energy of about 10 kcal/mole. However, because of the different experimental technique used, Chattopadhyay and Measor[8] were able to study the oxidation of Co at temperatures 50–60 K below our experimental limits. They found that as the temperature was lowered further, the activation energy for the rate constant K_0 continuously increased and at the lowest temperatures studied had a value of 18.5 kcal/mole—about the same activation energy as found above $T_{\epsilon-\gamma}$.

A comparison of the results from these two oxidation experiments clearly emphasizes the danger of analyzing rate date of any type from a relatively narrow temperature interval in terms of two Arrhenius laws with temperature *independent* activation energies. Such an analysis was previously made by us and others to discuss the changes in the oxidation rates of nickel,[4,5] iron,[2,7] and cobalt[6] near their Curie temperatures as well as the changes in the rate of nickel carbonyl production[14] near the Curie temperatures of some NiCu alloys. In all of these experiments the unphysically large differences in activation energy found near T_c (0.5–1.0 eV/atom) are most likely due to the persistence of non-Arrhenius behavior at temperatures 50–100 K below T_c.

Further support for this hypothesis is found in recent studies of the sublimation rate of cobalt near its Curie temperature. As was found originally by Khandros and Bogolyubov[12] and more recently by Sales *et al.*[13] there is an apparent change in the activation barrier for sublimation of 0.5–0.8 eV/atom at the Curie temperature of cobalt when the data are analyzed in terms of two Arrhenius laws with temperature independent activation energies. However, as was shown by Sales *et al.*[13] one can account quantitatively for the observed results with a simple mean-field model which incorporates into the sublimation process the temperature dependence of the magnetic contribution to the binding energy of a cobalt surface atom. In addition, this model demonstrates that in studying reaction rate anomalies near a ferromagnetic phase transition one should only expect *true* Arrhenius behavior at temperatures where the magnetization, $M(T)$, is approximately constant. For most ferromagnets this implies temperatures below about $0.6T_c$, where the magnetization has attained about 90% of its maximum value. In all of the experiments mentioned above the reaction rates were not measured at temperatures below about $0.85-0.90 \times T_c$.

Davies *et al.*[26] studied the oxidation rate of iron and found no anomaly in the parabolic rate constant k near $T_{\alpha-\gamma}$. However, in their experiments the *initial* oxidation process was not studied and k was determined from the growth rates of much thicker oxide layers. As can be seen from Fig. 8, the anomaly in the oxidation rate near $T_{\alpha-\gamma}$ decreases rapidly with increasing oxide thickness; hence it is not surprising that no anomaly was observed by these researchers.

B. Crystallographic versus magnetic phase transitions

The magnetic phase transformation of nickel and the crystallographic phase transformation of cobalt occur in a similar temperature range (573–773 K), and the oxide layers studied were of comparable thickness (~100 Å).[4] The magnetic and crystallographic phase transitions of iron also occur in a similar temperature interval (973–1273 K) and in both experiments oxide layers of about 100 000 Å were studied.[7] As was noted in the Introduction, it was hoped that by comparing the results from the nickel and cobalt oxidation experiments, and the results from the two iron oxidation experiments, some insight could be gained concerning the effects of a magnetic versus a crystallographic phase transition on metallic oxidation.

For the temperature ranges and oxide thicknesses encountered in the four oxidation experiments discussed above, previous work has established that only FeO, NiO, and CoO are formed.[19,26,27] All three oxides have a simple NaCl cubic crystal structure but form with a metal deficiency. The metal deficiency is known to be particularly high for Wüstite (FeO) and can easily exceed 5%.[26] Although there are some contradictory results for cobalt, the vast majority of

experimental evidence (radioactive tracer, inert marker, and cation substitution experiments) indicates that the growth of FeO, CoO, and NiO is primarily by outward diffusion of the metal cations (Fe^{2+}, Ni^{2+}, and Co^{2+})[28] through cation vacancies in the oxide.

Qualitatively, the growth of an oxide layer of FeO, CoO, or NiO can be divided into three spatially separate regions. At the metal-oxide interface there is a boundary reaction where metal atoms are incorporated into the oxide. At this interface the metal surface supplies to the growing oxide both positively charged metal ions and electrons.

At the oxygen-oxide interface there is another boundary reaction in which oxygen molecules dissociatively chemisorb to the oxide, trap electrons, and finally combine with metal ions to form more oxide. During this process the oxygen ions also create metal vacancies near the oxygen-oxide interface.

In the bulk oxide both metal ions and electrons (or metal vacancies and holes) migrate across the oxide driven by a concentration gradient of metal vacancies and by the electric field which must be present. The electric field can be regarded as the equalizing force which compensates for the inherently different mobilities of metal ions and electrons in a growing oxide. For example, as has been emphasized by Fromhold,[24] during oxide growth there can be no net transfer of charge (other than the charge necessary to set up the electric field). This implies that

$$j_i(E)q_i + j_e(E)q_e = 0 \ , \tag{4}$$

where $j_i(j_e)$ is the mass current density due to ionic (electronic) motion, $q_i(q_e)$ is the metal ion (electron) charge, and E is the electric field. Depending on the sign of E either the electronic or ionic current can be rate limiting. If the ionic movement through the oxide is intrinsically slower than the electronic motion, the net electric field will increase the ionic current and retard the electron current such that Eq. (4) is satisfied. In general, for thin oxide layers the effects of the boundary reactions and the electric fields are important, while for thicker oxide layers ionic and electronic diffusion become dominant.

With this simplified picture of metallic oxidation, a change in the crystal structure of the metal could affect the rate of oxidation by:

(i) Changing the number of metal atoms per cm^2 at the metal oxide interface, and/or the binding energy per surface atom. (This would modify the metal-oxide boundary condition.)

(ii) Altering the rate of thermionic emission of electrons into the oxide. [This would modify $j_e(E)$ in Eq. (4), which would change the electric field E and thus change $j_i(E)$ which is proportional to the rate of oxide growth.]

(iii) Modifying the stress induced in the growing oxide. [A slight expansion or contraction of the ox-

TABLE III. Difference in apparent activation energies for oxidation ΔE near the crystallographic or magnetic phase transition for different oxide thicknesses x_0.

Nickel (Ref. 4) (magnetic)		Cobalt (crystallographic)		Iron (Ref. 7) (magnetic)		Iron (crystallographic)	
ΔE (kcal/mole)	x_0 (Å)	ΔE (kcal/mole)	x_0 (Å)	ΔE (kcal/mole)	x_0 (10^5 Å)	ΔE (kcal/mole)	x_0 (10^5 Å)
−16.4	75	24.7	50	32	0.5	48.9	0.5
−21.3	95	18.2	100	−13.5	1.0	35.1	1.5
−24.8	115	11.6	200	−20.7	1.5	22.8	4.0
−28.8	140	3.1	500	−26.5	2.0	17.8	6.0

ide lattice would affect the diffusion coefficient of metal ions in the oxide.]

Similarly, a change in the magnetic phase of the metal could affect the rate of oxidation by:

(i) Changing the binding energy of a metal surface atom.

(ii) Modifying the rate of thermionic emission of electrons into the oxide.

(iii) Altering the stress induced in the growing oxide layer (near the Curie temperature there is appreciable expansion of the metal lattice).[29]

For "thin" oxide layers one can attribute the anomalies observed in the oxidation rates of Fe, Ni, or Co to one or more of the coupling mechanisms listed above. Experimentally, it is very difficult to separate the effects of one mechanism from another on the oxidation rate. However, it can be shown that these coupling mechanisms all become weaker for thicker oxide layers. That is, any anomaly in the oxidation rate due to one or more of the above mechanisms should become *smaller* with increasing oxide thickness. As can be seen from Figs. 4 and 8, the anomaly in the oxidation rate for Co near $T_{\epsilon-\gamma}$ does indeed diminish with increasing oxide thickness x_0.

Near the Curie temperature of Fe and Ni, however, our previous results showed that the anomaly in the oxidation rate near T_c actually *increased* with increasing oxide thickness. This is illustrated in Table III where values for the difference in the apparent activation energies for oxidation near the crystallographic or magnetic phase transition are shown for different values of x_0. These results indicate that there is a major qualitative difference between the effects of a crystallographic versus a magnetic phase transition on the oxidation kinetics of Fe, Ni, and Co. Since the coupling mechanisms listed above are similar for both types of phase transition, we suggest that the difference may be due to the spontaneous macroscopic magnetic field which develops below T_c when iron and nickel become ferromagnetic. Such a field could influence the motion of the charged metal ions and electrons in the oxide and might have an effect on the motion of the paramagnetic oxygen molecules near the oxide surface. Further oxidation experiments in carefully oriented external magnetic fields may be able to test this hypothesis.

ACKNOWLEDGMENT

This research was supported by the U.S. Department of Energy under Contract No. DE-AT03-76ER70227.

---

*Present address: Material and Molecular Research Division, Lawrence Berkeley Laboratory, University of California, Berkeley, Calif. 94720.

[1]H. H Uhlig, J. Pickett, and J. Macnairn, Acta Metal. 7, 111 (1959).

[2]J. C. Measor and K. K. Afzulpurkar, Philos. Mag. 10, 817 (1964).

[3]J. C. Rocaries and M. Rigaud, Scr. Metall. 5, 59 (1971).

[4]B. C. Sales and M. B. Maple, Phys. Rev. Lett. 39, 1636 (1977).

[5]B. C. Sales, M. B. Maple, and F. L. Vernon III, Phys. Rev. B 18, 486 (1978).

[6]B. Chatterjee, Thin Solid Films 41, 227 (1977).

[7]B. C. Sales, A. L. Cabrera, and M. B. Maple, Solid State Commun. 30, 119 (1979).

[8]B. Chattopadhyay and J. C. Measor, J. Mater. Sci., 4, 457 (1969).

[9]R. J. H. Voorhoeve, in *Magnetism and Magnetic Materials—1973 (Boston)*, edited by C. D. Graham and J. J. Rhyne, AIP Conf. Proc. No. 18 (AIP, New York, 1974), Part I, p. 19.

[10]G. Parravano, J. Chem. Phys. 20, 342 (1952).

[11]A. L. Cabrera, B. C. Sales, M. B. Maple, H. Suhl, G. W. Stupian, and A. B. Chase, Mater. Res. Bull. 14, 1155 (1979).

[12]V. O. Khandros and N. A. Bogolyubov, Sov. Phys. Solid State 14, 1592 (1972) [Fiz. Tverd. Tela (Leningrad) 14, 1837 (1972)].

[13]B. C. Sales, J. E. Turner, and M. B. Maple, Phys. Rev. Lett. 44, 586 (1980).

[14]R. S. Mehta, M. S. Dresselhaus, G. Dresselhaus, and H. J. Zeiger, Phys. Rev. Lett. 43, 970 (1979).

[15]P. K. Gallagher, E. M. Gyorgy, and H. E. Bair, J. Chem. Phys. 71, 830 (1979).

[16]H. Suhl, Phys. Rev. B 11, 2011 (1975).

[17]H. Suhl, in *The Physical Basis for Heterogeneous Catalysis*, edited by E. Drauglis and R. I. Jaffee (Plenum, New York, 1975), pp. 427–435.

[18]O. S. Edwards and H. Lipson, J. Inst. Met. 69, 177 (1943).

[19]E. A. Gulbransen and K. F. Andrew, J. Electrochem. Soc. 98, 242 (1951).

[20]K. Hauffe, *Oxidation of Metals* (Plenum, New York, 1965).

[21]O. Kubaschewski and B. F. Hopkins, *Oxidation of Metals and Alloys* (Butterworths, London, 1962).

[22]F. P. Fehlner and N. F. Mott, Oxid. Met. 2, 59 (1970).

[23]K. R. Lawless, Rep. Prog. Phys. 37, 231 (1974).

[24]A. T. Fromhold, Jr., *Theory of Metal Oxidation* (North-Holland, New York, 1976), Vol. I.

[25]We note that B. Chatterjee [Solid State Commun. 27, 1455 (1978)] claims that our measured nickel oxidation isotherms (Refs. 4 and 5) are better described by a direct logarithmic law than a power law. To this claim we have two comments. First, only about the first third of each isotherm (one-third of the data) can be adequately described by a logarithmic growth law. Second, the theory of Chattopadhyay [Thin Solid Films 16, 117 (1973)] used by Chatterjee to analyze in detail the oxidation kinetics of Ni, Fe, and Co contains an invalid approximation. Without commenting on the physical assumptions used to construct the theory, the following approximation for the

space charge potential, V_p, is made: $V_p = 4\pi n_v e(\gamma y + \frac{1}{2}y^2)/\epsilon \approx 4\pi n_v e \gamma y/\epsilon$ on the grounds that the oxide thickness y is small and the term in y^2 can be neglected. In the equation for V_p, $n_v e$ is the space charge density, ϵ is the dielectric constant of the oxide, and γ is the thickness of the dipole surface charge layer ($\gamma \approx 3$ Å). Since γ is so small, however, $\frac{1}{2}y^2 > \gamma y$ for oxides thicker than 6 Å, and a logarithmic growth law does not follow.

[26]M. H. Davies, M. T. Simnad, and C. E. Birchenall, Trans. Metall. Soc. AIME 191, 889 (1951).
[27]O. Kubaschewski and B. E. Hopkins, *Oxidation of Metals and Alloys* (Butterworths, London, 1962), p. 243.
[28]O. Kubaschewski and B. E. Hopkins, *Oxidation of Metals and Alloys* (Butterworths, London, 1962), Chap. 4.
[29]T. G. Kollie, Phys. Rev. B 16, 4872 (1977).